Progress In Electromagnetics Research C, Vol. 125, 191–200, 2022

A Compact Folded RFID Tag Antenna with Nested Deformable Rings for Two-Side Anti-Metal Application

Chenchen Niu, Jiade Yuan*, and Zhimeng Xu

Abstract—A novel compact two-side anti-metal tag antenna for radio frequency identification (RFID) applications is proposed in this paper. The proposed tag antenna is composed by three aluminum patches separated by two layers of foam substrates. Particularly, the middle patch of the antenna is designed as three nested deformable rings for the miniaturization of antenna and realizes better power transmission coefficient (PTC) between the antenna and tag microchip. The antenna operates at the center frequency of 915 MHz and maintains a compact size of $35\,\text{mm} \times 22\,\text{mm} \times 2.15\,\text{mm}$ ($0.1068\lambda_0 \times 0.0671\lambda_0 \times 0.0066\lambda_0$). When the front or back side of the tag antenna is mounted on a large background metallic plate and tested with an effective-isotropic-radiated-power (EIRP) of 4 W, the antenna can achieve the maximum read distances of 6.23 m or 6.08 m. The tag antenna shows various advantages, including small size, low profile, and good antenna performance. Most importantly, the proposed tag antenna has two-side anti-metal property compared to a traditional single-side anti-metal antenna, which fulfills the emerging demands in the industrial internet of things field.

1. INTRODUCTION

Radio frequency identification (RFID) technology is a non-contact automatic identification technology. Ultra-high frequency (UHF) RFID systems have been widely used in logistics warehousing, asset management, medical equipment, and other fields due to their fast read rate, high capacity, and long-term storage [1, 2]. Nevertheless, when the tag is placed in close proximity to metallic objects, the image current induced on the metallic surface is 180° out-of-phase, which can significantly degrade antenna performance [3–5]. Therefore, it is a challenge to specially design the tag antenna in metallic environments.

Various methods have been proposed to ensure the stable operation of tag antennas in metallic surfaces. High-dielectric substrates [6] can meet the requirements of tags to work flexibly for different metallic objects. Insertion of electromagnetic band gap (EBG) [7, 8] or artificial magnetic conductor (AMC) [9, 10] can also mitigate the metal-to-tag impact. The microstrip antenna [11] is widely used in various metallic environments because the ground can isolate the radiating patch from the backing metal. To miniaturize the size, the designs of the planar inverted-F antenna (PIFA) [12–15] and planar inverted-L antenna (PILA) [16] have been carried out by shorting one edge of its radiator to ground. Some special structures have also been used to design various on-metal tag antennas, such as complementary split ring resonator (CSRR) [17], double loop structure [18], and half-wavelength slot resonator [19]. Furthermore, several folded patch antennas [20–25] have been used for designing the anti-metal tags, which not only simplifies the fabrication complexity, but also increases the flexibility of antenna tuning. The antenna performance can be optimized by simply adjusting structures, such as radiating patches, shorting stubs, shorting walls, and grounds.

The above mentioned tag antennas are one-side anti-metal antennas that must be placed on the metallic plate with a specific side. In this paper, we propose a two-side anti-metal tag antenna. The

Received 6 September 2022, Accepted 14 October 2022, Scheduled 21 October 2022
* Corresponding author: Jiade Yuan (yuanjiade@fzu.edu.cn).
The authors are with the College of Physics and Information Engineering, Fuzhou University, Fuzhou, Fujian, China.

two-side anti-metal feature is realized by adopting a three-layer folded metal patch, in which three nested deformable rings are designed in the middle layer for the miniaturization of antenna.

2. ANTENNA STRUCTURE AND ANALYSIS

2.1. Antenna Structure

The proposed tag antenna is obtained by folding a single-side rectangular naked inlay twice. As shown in Figure 1(b), it comprises three conducting layers separated by two layers of foam substrates. As shown in Figure 1(b) and Figure 1(c), the three conducting layers are named as conducting layer A, conducting layer M, and conducting layer B, respectively. The conducting layer A and conducting layer B are both complete rectangular patches with a size of 35 mm × 22 mm. The conducting layer M is composed of three nested deformable rings, namely outer deformable ring, middle deformable ring, and inner deformable ring, as shown in Figure 1(a). Furthermore, as shown in Figure 1(c), the conducting

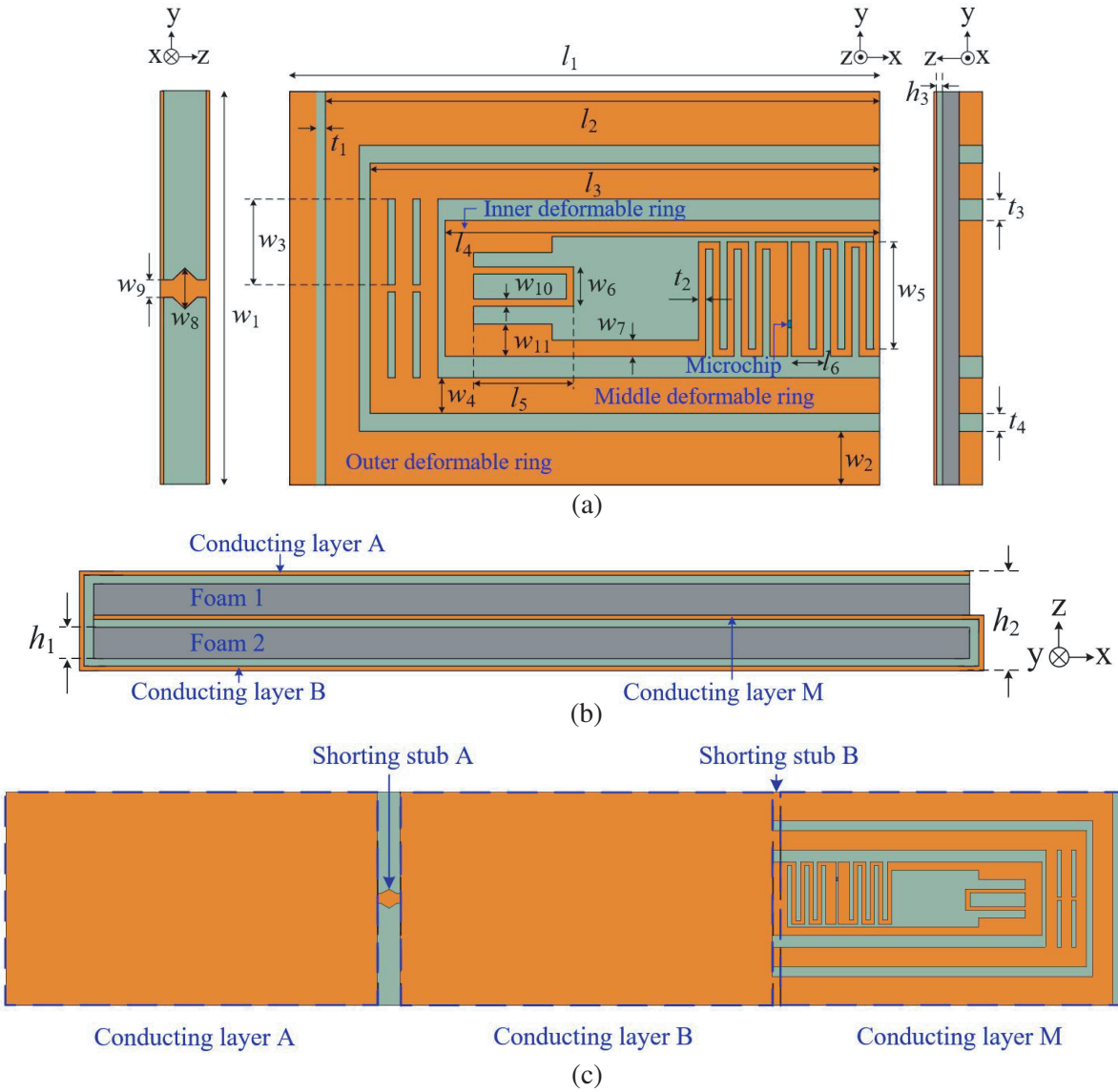

Figure 1. Configuration of the proposed tag antenna. (a) The conducting layer M and side views of the proposed tag antenna. (b) Cross-sectional view. (c) Naked inlay of the proposed tag antenna.

layer A is connected to the conducting layer B by the shorting stub A on the left side of the tag antenna, and the conducting layer M is connected to the conducting layer B by the shorting stub B on the right side of the tag antenna. Two pieces of soft polyethylene foams, namely foam 1 and foam 2, with $\varepsilon_r = 1.06$ and $\tan\delta = 0.0001$, are inserted in the proposed antenna as the substrate.

The conducting layer M is designed as three nested deformable rings, wherein the outer and middle deformable rings are both U-shaped, and the inner deformable ring is annular. The tag microchip is MW8112 of MAXWAVE MICRO Co., Ltd and located at the junction of two meander arms of the inner deformable ring. The input impedance of the microchip at 915 MHz is 18-j253 Ω, and the read sensitivity is −20 dBm. When the proposed tag is placed on a metallic object, the conducting layer touching background metallic plate is considered as the ground, and the other two conducting layers can be regarded as the radiating layer. In all simulations and measurements of the tag, the tag antenna is positioned at the center of a 200 mm × 200 mm metallic plate performing as a metallic background.

2.2. Design Analysis

The proposed tag antenna is evolved from a simple nested ring antenna. Figure 2 shows the evolution: a simple nested ring antenna of Figure 2(a) to the meandered arms structure of Figure 2(b), then loading the shorting stub B of Figure 2(c), and finally the proposed structure of Figure 2(d). Only the conducting layer M and shorting stub B are shown in Figure 2 because other parts of the antenna are unchanged during the evolution. In Figure 2(b), the inner ring is etched a rectangular conductor on the left side, forming a rectangular conductor ring on the left side and forming two meandered arms on the right side. In Figure 2(c), the rectangular shorting wall on the right side is replaced by the shorting stub B. Finally, in Figure 2(d), four notches and a stripline are etched on the left side in the middle and outer ring, respectively. All evolution parts are marked with lines in Configurations II–IV.

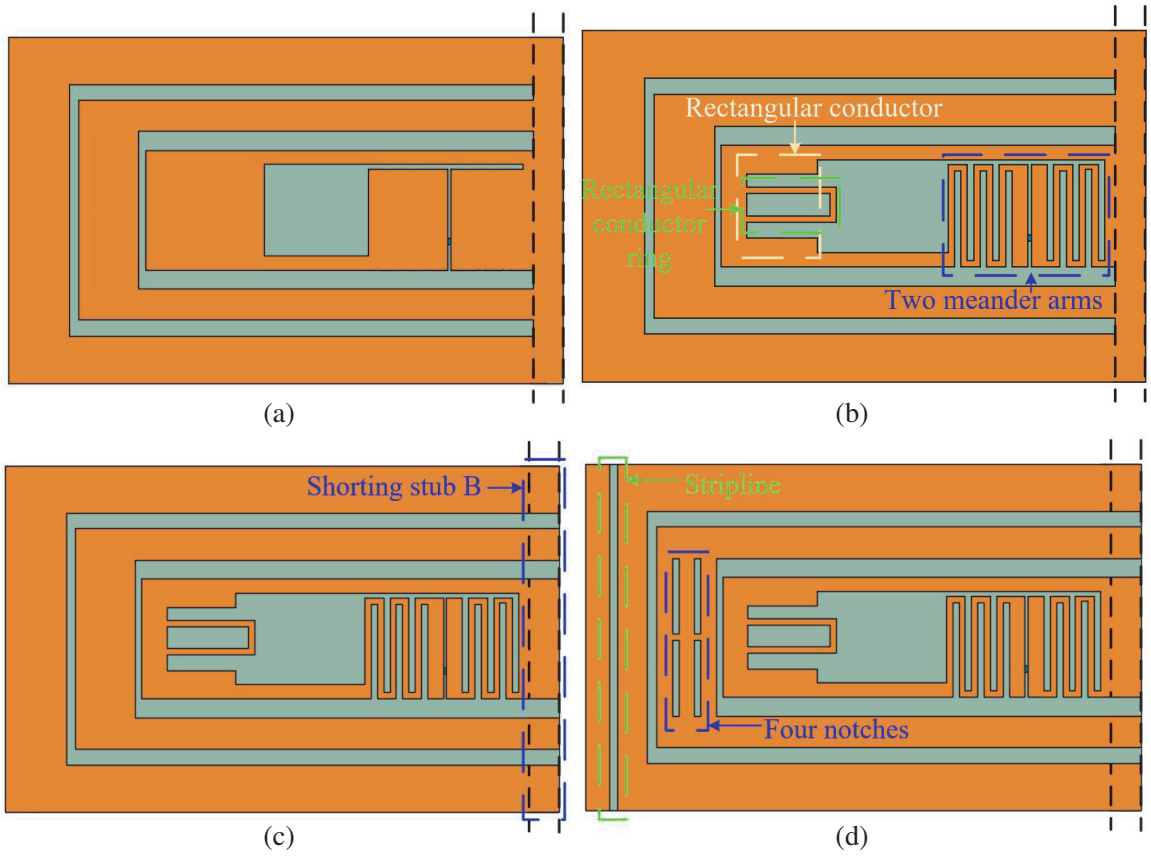

Figure 2. Intermittent tag configurations of the proposed tag antenna. (a) Configuration I. (b) Configuration II. (c) Configuration III. (d) Configuration IV.

The power transmission coefficient (PTC) is used to measure the impedance matching between the tag antenna and tag microchip. During the evolution of the antenna from Configuration I to Configuration IV, the frequency corresponding to the maximum PTC gradually approaches the same, as shown in Figure 3. In this paper, when the conducting layer B is placed to touch the background metallic plate, the conducting layers A and M act as radiators, named as CLA status. Similarly, when the conducting layer A is placed to touch the background metallic plate, the conducting layers M and B act as radiators, named as CLB status.

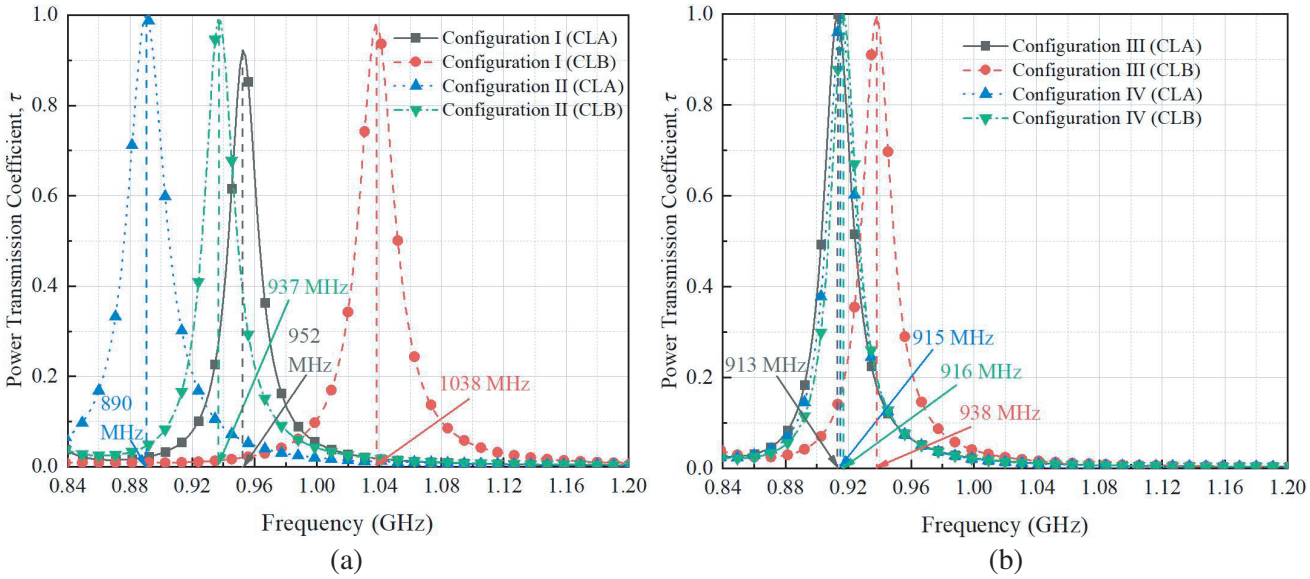

Figure 3. Power transmission coefficients of tag antennas with different structures. (a) PTCs of structure I and structure II. (b) PTCs of structure III and structure IV.

The frequencies corresponding to the maximum PTC for the CLA and CLB curves of Configuration I are 952 MHz and 1038 MHz, respectively, and the corresponding frequency difference is 86 MHz. For Configuration II, the frequencies corresponding to the maximum PTC are 890 MHz (CLA) and 937 MHz (CLB), respectively. The corresponding frequency difference is reduced to 47 MHz, as shown in Figure 3(a). The reason can be explained as that the inner deformable ring is effectively coupled to other metal rings, and the corresponding inductance becomes slightly larger.

In order to further reduce the difference of the frequencies corresponding to the maximum PTC, the shorting stub B is introduced and optimized, as shown in Figure 2(c). For Configuration III, the frequencies corresponding to the maximum PTC can be tuned to 913 MHz (CLA) and 938 MHz (CLB), respectively. The corresponding frequency difference is further reduced to 25 MHz. The reason can be explained as that Configuration III can be regarded as extending the length of the three deformable rings, and the inductance of the antenna is increased.

Finally, the outer and middle deformable rings of the antenna are optimized. The increased stripline slot and four notches can improve the capacitive coupling, as shown in Configuration IV of Figure 2(d). The frequencies corresponding to the maximum PTC are 915 MHz (CLA) and 916 MHz (CLB), respectively. The corresponding frequency difference is only 1 MHz. At this time, whether conducting layer A or conducting layer B touches the background metal plate, the working performance of the proposed antenna is nearly the same. It is worth mentioning here that the maximum PTCs are all able to maintain ≥ 0.98 for the curves in Figure 3(b).

The proposed tag antenna is simulated and optimized using HFSS. In the design process, several design parameters ($l_1 = 35$ mm, $w_1 = 22$ mm, $h_1 = 1$ mm, and $h_3 = 0.05$ mm) are fixed, while others are obtained through the optimization processes. By setting the impedance and realized gain as the objective functions, the optimization processes will be automatically halted as soon as the functions are met. After several iterations, the optimized parameters are shown in Table 1.

Table 1. The optimized design parameters of the proposed tag antenna.

Parameter	Dimension (mm)	Parameter	Dimension (mm)	Parameter	Dimension (mm)	Parameter	Dimension (mm)
l_1	35	w_1	22	w_7	0.9	h_2	2.15
l_2	31	w_2	3	w_8	2	h_3	0.05
l_3	28.5	w_3	4.8	w_9	1	t_1	0.5
l_4	24.3	w_4	2	w_{10}	0.4	t_2	0.4
l_5	5.6	w_5	6	w_{11}	1.8	t_3	1.2
l_6	1.8	w_6	2.2	h_1	1	t_4	1

3. PARAMETRIC ANALYSIS

Parametric analyses have been conducted to optimize the proposed tag antenna. Only the mentioned parameters are changed, and other parameters remain unchanged at a time.

3.1. Variation of Stripline Width t_1 and Notch Length w_3

The variations of the impedance and power transmission coefficient of the antenna with the stripline width (t_1) and notch length (w_3) are analyzed. As shown in Figures 4(a)–4(b) and Figures 4(d)–4(e), the impedance gradually decreases with the increasing t_1 and w_3 in the frequency range of 880 MHz–980 MHz. With increasing t_1 and w_3, the frequencies corresponding to the maximum PTC are shifted

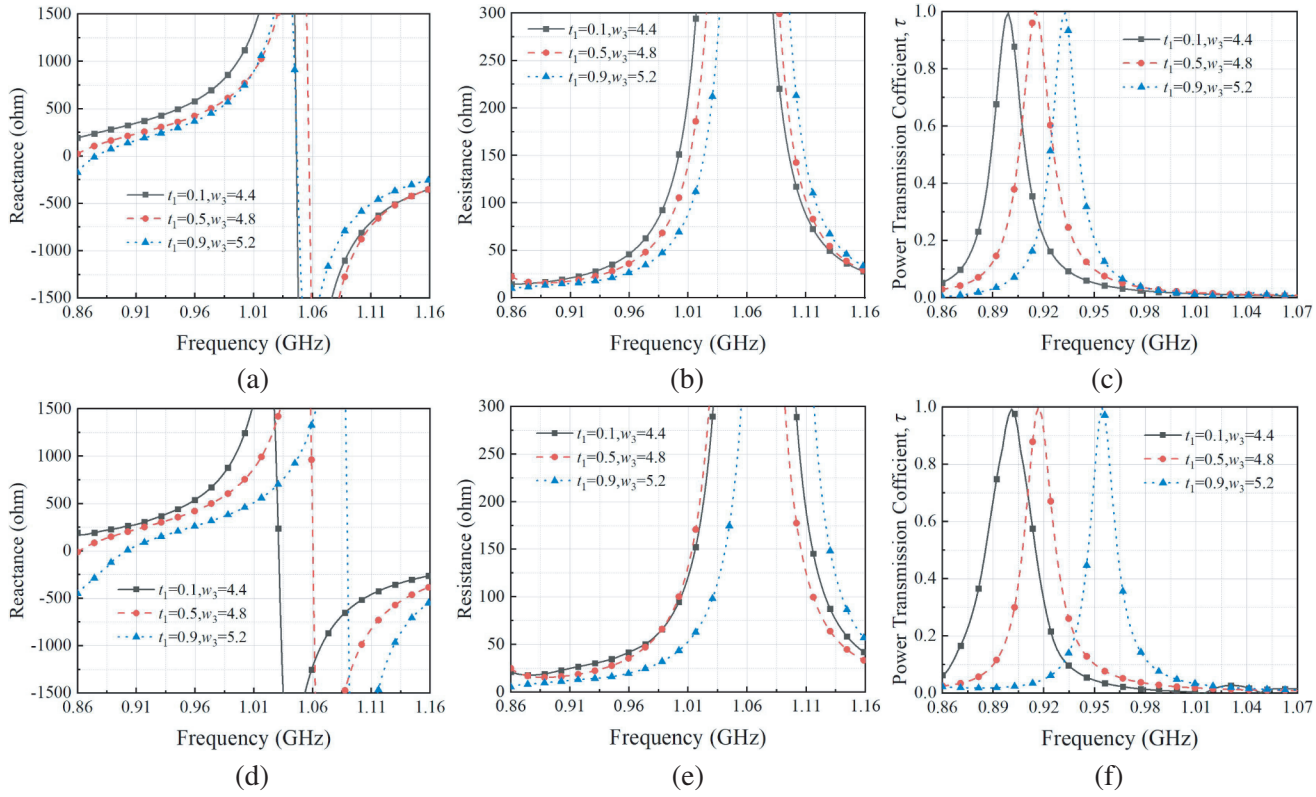

Figure 4. Effects of changing t_1 and w_3 on the (a) reactance (CLA), (b) resistance (CLA), (c) PTC (CLA), (d) reactance (CLB), (e) resistance (CLB), and (f) PTC (CLB).

to high frequencies for both CLA and CLB statuses, as shown in Figures 4(c) and 4(f). The reason can be explained as that increasing t_1 and w_3 will reduce the inductive reactance of the tag antenna, thereby increasing the resonant frequency.

3.2. Variation of Rectangular Length l_5 and Meander Arm Length w_5

The variations of the impedance and power transmission coefficient of the antenna with the rectangular length (l_5) and the meandered arm width (w_5) are analyzed. As shown in Figures 5(a)–5(b) and Figures 5(d)–5(e), the impedance shows an increase with the increasing l_5 and w_5 in the frequency range of 880 MHz–1000 MHz. With increasing l_5 and w_5, the frequencies corresponding to the maximum PTC are shifted to low frequencies for both CLA and CLB statuses, as shown in Figures 5(c) and 5(f). The reason can be explained as that increasing l_5 and w_5 can increase the current length, thereby decreasing the resonant frequency.

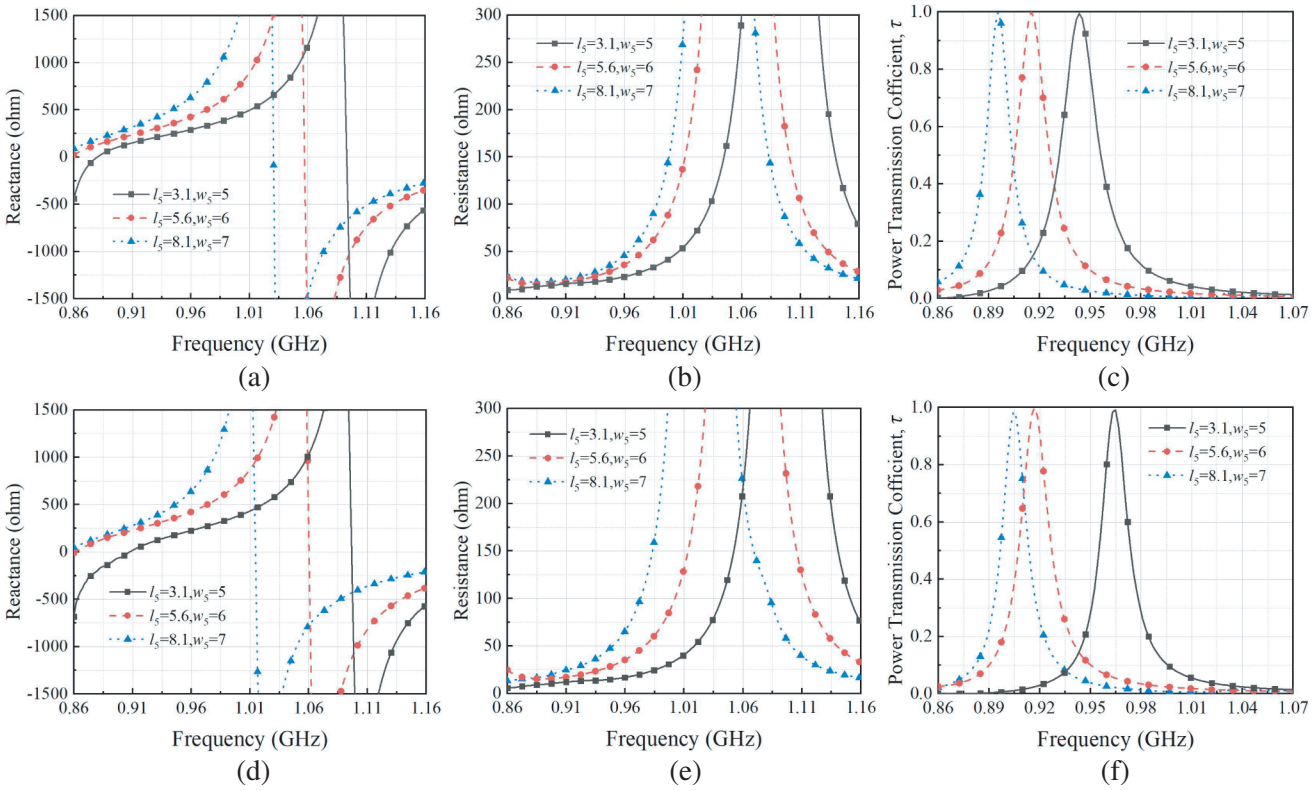

Figure 5. Effects of changing l_5 and w_5 on the (a) reactance (CLA), (b) resistance (CLA), (c) PTC (CLA), (d) reactance (CLB), (e) resistance (CLB), and (f) PTC (CLB).

4. RESULTS AND DISCUSSION

Figure 6 demonstrates the structural view after being folded (upper part), and the fabricated naked inlay (lower part). The proposed tag antenna is measured with the Voyantic Tagformance measurement system, as shown in Figure 7. This measured system includes a linearly polarized reader antenna that is used for transmitting signals and receiving the backscattered signals from the tag antenna. The reader antenna is fixed at a constant distance along the z-axis from the tag antenna. The effective-isotropic-radiation-power (EIRP) is fixed at 4 W for all of the subsequent measurements.

The simulated and measured realized gains of the tag antenna are plotted in Figure 8(a). For the CLA status, the maximum simulated realized gain is −4.93 dB at 915 MHz, and the maximum measured realized gain of −6.06 dB is found at 910 MHz. Similarly, for the CLB status, the maximum simulated

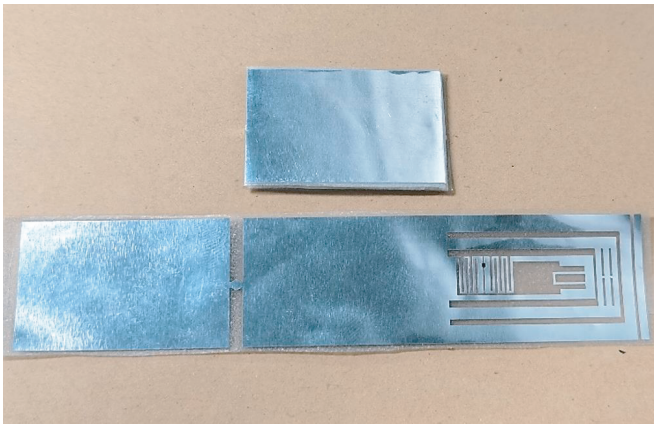

Figure 6. Assembled tag antenna (upper part) and naked inlay of the proposed tag antenna (lower part).

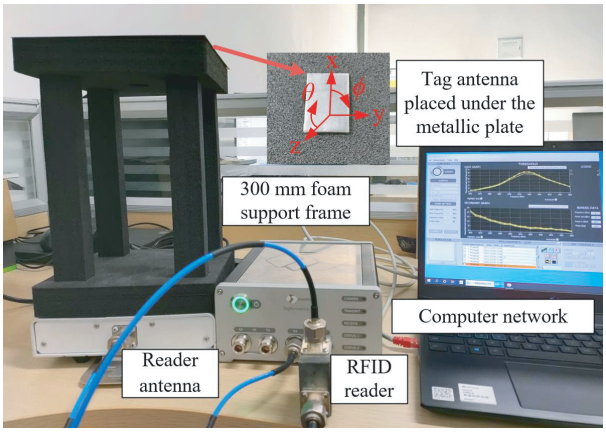

Figure 7. Tag antenna measurement setup of Voyantic Tagformance.

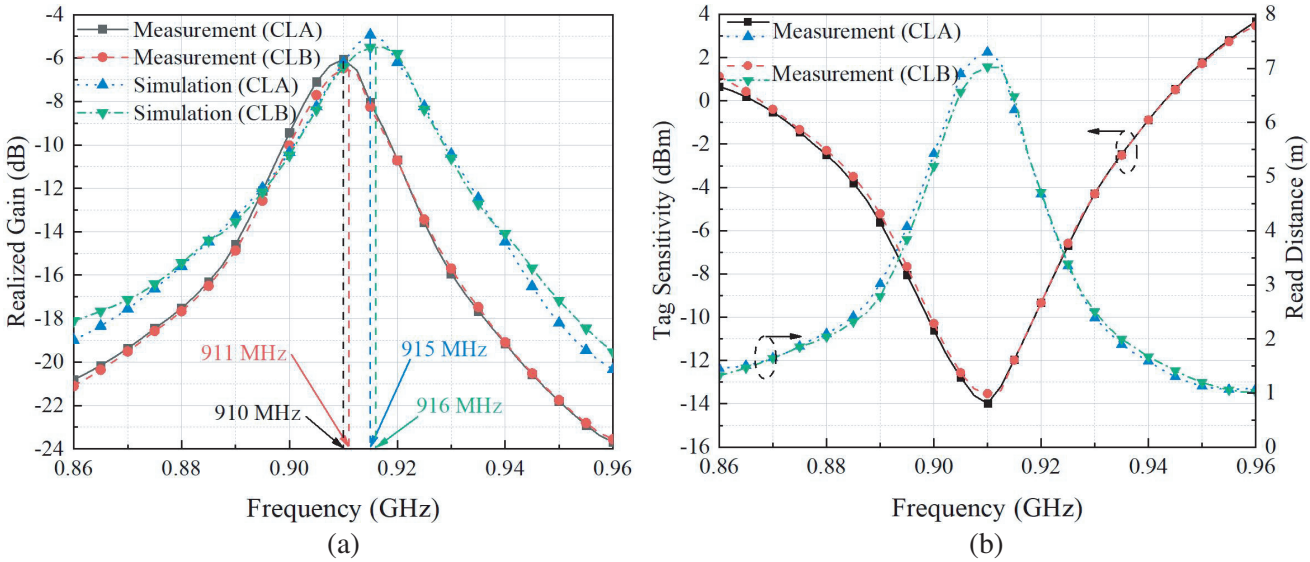

Figure 8. (a) Measured and simulated realized gains of the proposed tag antenna. (b) Measured tag sensitivities and measured read distances of the proposed tag antenna.

realized gain is −5.47 dB at 916 MHz, and the maximum measured realized gain of −6.46 dB is found at 911 MHz. In general, the maximum measured realized gains are 1.13 dB and 0.99 dB lower than the simulation results, respectively. At the same time, the frequency values corresponding to the maximum gain are about 5 MHz offset between simulated and measured results. The deviations can be due to antenna fabrications, measurement errors, and chip impedance variations.

As can be seen in Figure 8(b), the maximum measured tag sensitivities of −13.98 dBm and −13.52 dBm are found at 910 MHz and 911 MHz for the CLA status and CLB status, respectively. Here, the frequencies of 910 MHz and 911 MHz are considered the measured resonant frequencies for the CLA status and CLB status, respectively. The read distance (r) of the tag can be computed using Equation (1):

$$r = \frac{\lambda}{4\pi}\sqrt{\frac{P_{\text{EIRP}}G_r\tau}{P_{th}}} \tag{1}$$

where P_{EIRP} is the maximum permissible equivalent isotropic radiated power transmitted by the reader,

G_r the realized gain of the proposed tag antenna, τ the power transmission coefficient, and P_{th} the minimum activation power to be received by the microchip. It should be mentioned that the default P_{EIRP} of the Voyantic Tagformance is 3.28 W, which is used for calculating the measured read distance. To calculate the read distance with reference to P_{EIRP} of 4 W, the equation is required to express as:

$$r = d_{\max}\sqrt{\frac{P_{\text{EIRP(max)}}}{P_{\text{EIRP(ref)}}}} \tag{2}$$

where $d_{\max}$ is the read distance under the condition of $P_{\text{EIRP}} = 3.28\,\text{W}$, $P_{\text{EIRP(max)}} = 4\,\text{W}$, and $P_{\text{EIRP(ref)}} = 3.28\,\text{W}$. As can be seen in Figure 8(b), the tag achieves a maximum measured read distance of 7.29 m at 910 MHz, and the measured read distance of 6.23 m is found at 915 MHz for the CLA status. Similarly, the tag can achieve a maximum measured read distance of 7.02 m at 911 MHz and the measured read distance of 6.08 m at 916 MHz for the CLB status. The discrepancies between the measurement and simulation may be caused by fabrication errors and experimental tolerances.

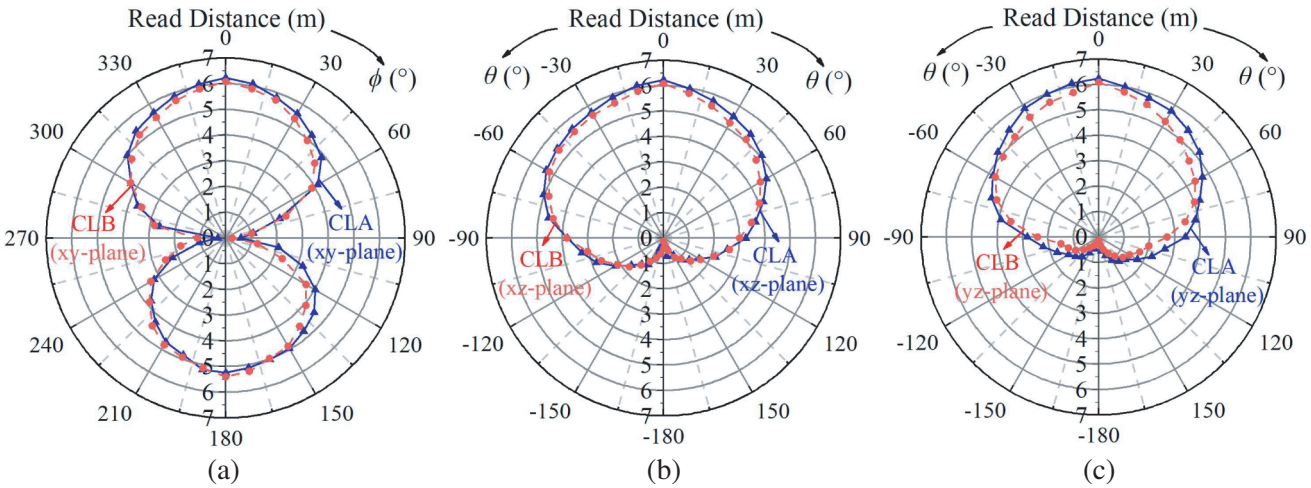

Figure 9. Measured read distances of the proposed tag antenna in the (a) xy-plane at 915 MHz, (b) xz-plane at 915 MHz, and (c) yz-plane at 915 MHz.

Table 2. Performances comparison between several UHF metal-mountable tags.

Ref.	Tag Dimenion (mm)	Flexibility	Substrate Permittivity (ε_r)	No. of Usable Sides	Backing Metal Size (mm)	Realized Gain (dB)	Max. Read Distance (m)*
[6]	32 (diameter) × 1.5	Yes (ceramic)	12	1	100 × 100	−14.4	3.3
[17]	45 × 45 × 1.27	No (RO3010)	10.2	1	200 × 300	−4.6	9.1
[23]	40 × 40 × 1.6	Yes (foam)	1.06	1	200 × 200	−10	5.5
[24]	23 × 16 × 1.6	Yes (foam)	1.06	1	200 × 200	−10.3	4.5
[22]	40 × 25 × 3	Yes (foam)	1.03	1	200 × 200	−2.23	12.8
[25]	30 × 30 × 3	Yes (foam)	1.03	1	200 × 200	−4.35	10
This work	35 × 22 × 2.15	Yes (foam)	1.06	2	200 × 200	−6.06 and −6.46	5.64 and 5.51

*Max. Read Distance is calculated based on microchip's read sensitivity of −20 dBm and an EIRP power of 4 W.

In Figure 9, the measured read distance patterns of the prototype tag antenna in the xy-, xz-, and yz-planes at 915 MHz are shown, respectively. As depicted in Figure 9(a), the angle range of reading distance exceeding 4 m is $295° \leq \phi \leq 60°$ and $120° \leq \phi \leq 225°$ in the xy-plane for the CLA status, while the angle range of reading distance exceeding 4 m is $296° \leq \phi \leq 58°$ and $131° \leq \phi \leq 227°$ in the xy-plane for the CLB status. Moreover, the angle range of reading distance exceeding 4 m is around 150° for CLA and CLB statuses in the xz-plane and yz-plane, as shown in Figures 9(b) and 9(c).

Table 2 shows the comparison between the proposed tag antenna and some of the recently reported metal-mountable UHF tag antennas. To make the comparison easier, the read distances of all the tags are recalculated and re-calibrated using a fixed reader power ($P_{\text{EIRP}} = 4$ W) and a constant microchip sensitivity ($P_{ic} = -20$ dBm). Compared with the antennas described in [6] and [24], the proposed tag antenna has higher realized gains. Compared with the antenna described in [17], the proposed tag antenna has a lower cost and can be easily fabricated. Compared with the antennas described in [22] and [23], the proposed tag antenna has a smaller volume. Compared with the antenna described in [25], the proposed tag antenna has a low profile. The most important thing is that the antenna designed in this paper can achieve two-side anti-metal performance.

5. CONCLUSION

A compact two-side anti-metal tag antenna is studied in this paper. The antenna is composed of three aluminum patches separated by two layers of foam substrates and can be easily fabricated by folding a single-sided rectangular naked inlay twice. The effects of the variation of some structural parameters on the antenna performance are discussed. The antenna gain, tag sensitivity, and reading distance are measured using the Voyantic Tagformance measurement system. The proposed antenna is compared with the antennas in the recent published paper and demonstrates the advantages over other compared antennas, especially for the two-side anti-metal feature. The proposed tag antenna can achieve better read distances under the requirements of small size, low profile, and low cost, which can be well applied in the industrial internet of things.

ACKNOWLEDGMENT

This work was supported in part by the National Natural Science Foundation of China (62071125) and the Science and Technology Innovation Project Plan of Fuzhou of China (2021-P-029).

REFERENCES

1. Yan, Z., S. Lu, and C. Zhang, "Design and implementation of long-distance dual PIFA antenna structure of small embedded metal UHF RFID tag," *Progress In Electromagnetics Research C*, Vol. 116, 95–112, 2021.
2. Chiang, S. M., T. L. Lee, E. H. Lim, P. S. Chee, Y. H. Lee, F. L. Bong, Y. N. Phua, and B. K. Chung, "Miniature folded dipole in rotational symmetry for metalTag design," *Progress In Electromagnetics Research C*, Vol. 110, 55–66, 2021.
3. Fei, Y. and J. Zhi, "A broadband UHF RFID tag antenna design for metallic surface using module matching," *Progress In Electromagnetics Research Letters*, Vol. 95, 83–90, 2021.
4. Yan, Y., J. Ouyang, X. Ma, R. Wang, and A. Sharif, "Circularly polarized RFID tag antenna design for metallic poles using characteristic mode analysis," *IEEE Antennas Wireless Propag. Lett.*, Vol. 18, No. 7, 1327–1331, July 2019.
5. Ma, Y. T., H. F. Ning, W. J. Meng, and C. L. Tian, "Design and evaluation of a planar I-shaped folded-patch antenna for compact passive UHF RFID tags to cohere on metal," *Progress In Electromagnetics Research Letters*, Vol. 94, 49–55, 2020.
6. Babar, A. A., T. Bjorninen, V. A. Bhagavati, L. Sydanheimo, P. Kallio and L. Ukkonen, "Small and flexible metal mountable passive UHF RFID tag on high-dielectric polymer-ceramic composite substrate," *IEEE Antennas Wireless Propag. Lett.*, Vol. 11, 1319–1322, November 2012.

7. Gao, B. and M. M. F. Yuen, "Passive UHF RFID packaging with Electro-magnetic Band Gap (EBG) material for metallic objects tracking," *IEEE Trans. Compon. Packag. Manuf. Technol.*, Vol. 1, No. 8, 1140–1145, August 2011.
8. Li, X., G. Gao, H. Zhu, Q. Li, and N. Zhang, "UHF RFID tag antenna based on the DLS-EBG structure for metallic objects," *IET Microw., Antennas Propag.*, Vol. 14, No. 7, 567–572, 2020.
9. Kim, D. and J. Yeo, "Dual-band long-range passive RFID tag antenna using an AMC ground plane," *IEEE Trans. Antennas Propag.*, Vol. 60, No. 6, 2620–2626, June 2012.
10. Ripin, N., E. Lim, F. Bong, and B. Chung, "Miniature folded dipolar patch with embedded AMC for metal mountable tag design," *IEEE Trans. Antennas Propag.*, Vol. 68, No. 5, 3525–3533, May 2020.
11. Ukkonen, L., M. Schaffrath, D. W. Engels, L. Sydänheimo, and M. Kivikoski, "Operability of folded microstrip patch-type tag antenna in the UHF RFID bands within 865–928 MHz," *IEEE Antennas Wireless Propag. Lett.*, Vol. 5, 414–417, August 2006.
12. Lin, K. H., S. L. Chen, and R. Mittra, "A looped-bowtie RFID tag antenna design for metallic objects," *IEEE Trans. Antennas Propag.*, Vol. 61, No. 2, 499–505, February 2013.
13. Michel, A., R. Colella, G. A. Casula, P. Nepa, L. Catarinucci, G. Montisci, G. Mazzarella, and G. Manara, "Design considerations on the placement of a wearable UHF-RFID PIFA on a compact ground plane," *IEEE Trans. Antennas Propag.*, Vol. 66, No. 6, 3142–3127, June 2018.
14. Zhang, J. and Y. Long, "A novel metal-mountable electrically small antenna for RFID tag applications with practical guidelines for the antenna design," *IEEE Trans. Antennas Propag.*, Vol. 62, No. 11, 5820–5829, November 2014.
15. Son, H.-W. and S.-H. Jeong, "Wideband RFID tag antenna for metallic surfaces using proximity-coupled feed," *IEEE Antennas Wireless Propag. Lett.*, Vol. 10, 377–380, April 2011.
16. Alja'afreh, S. S., Y. Huang, L. Xing, Q. Xu, and X. Zhu, "A low-profile and wideband PILA-based antenna for handset diversity applications," *IEEE Antennas Wireless Propag. Lett.*, Vol. 114, 923–926, April 2015.
17. Zuffanelli, S., G. Zamora, F. Paredes, P. Aguila, F. Martin, and J. Bonache, "On-metal UHF-RFID passive tags based on complementary split-ring resonators," *IET Microw. Antennas, Propag.*, Vol. 11, No. 7, 1040–1044, June 2017.
18. Li, H., J. Zhu, and Y. Yu, "Compact single-layer RFID tag antenna tolerant to background materials," *IEEE Access*, Vol. 5, 21070–21079, September 2017.
19. Lin, Y., M. Chang, H. Chen, and B. Lai, "Gain enhancement of ground radiation antenna for RFID tag mounted on metallic plane," *IEEE Trans. Antennas Propag.*, Vol. 64, No. 4, 1193–1200, April 2016.
20. Ng, W. H., E. H. Lim, F. L. Bong, and B. K Chung, "Compact folded crossed-dipole for on-metal polarization diversity UHF tag," *IEEE J. Radio Freq. Identif.*, Vol. 4, No. 2, 115–123, June 2020.
21. Lee, Y. H., E. H. Lim, F. L. Bong, and B. K. Chung, "Compact folded C-shaped antenna for metal-mountable UHF RFID applications," *IEEE Trans. Antennas Propag.*, Vol. 67, No. 2, 765–773, February 2019.
22. Moh, C. W., E. H. Lim, F. L. Bong, and B. K. Chung, "Miniature coplanar-fed folded patch for metal mountable UHF RFID tag," *IEEE Trans. Antennas Propag.*, Vol. 66, No. 5, 2245–2253, May 2018.
23. Ng, W. H., E. H. Lim, F. L. Bong, and B. K. Chung, "Folded patch antenna with tunable inductive slots and stubs for UHF tag design," *IEEE Trans. Antennas Propag.*, Vol. 66, No. 6, 2799–2806, June 2018.
24. Bong, F. L., E. H. Lim, and F. L. Lo, "Miniaturized dipolar patch antenna with narrow meandered slotline for UHF tag," *IEEE Trans. Antennas Propag.*, Vol. 65, 4435–4442, September 2017.
25. Bong, F. L., K. Thirappa, E. H. Lim, and K. Perumal, "Compact metal-mountable UHF RFID tag antenna with two large C-shaped slots for on-the-fly tuning," *Progress In Electromagnetics Research M*, Vol. 101, 173–183, 2021.